Electrical Double Layer Spillover Drives Coupled Electron- and Phase- Transfer Reactions at Electrode/Toluene/Water Three-Phase Interfaces

Andrew D. Pendergast, Salvador Gutierrez-Portocarrero, Rodrigo Noriega*, and Henry S. White*

Department of Chemistry, University of Utah, Salt Lake City, UT 84112, USA

*To whom correspondence should be addressed: noriega@chem.utah.edu, white@chem.utah.edu, white@chem.utah.edu,

Abstract

A mechanism for the concerted pathway of coupled electron- and phase-transfer reactions (CEPhT) is proposed. The driving force for CEPhT at three-phase interfaces formed by a solid electrode, an insulating organic solvent, and an aqueous electrolyte is caused driven by electric double layer (EDL) spillover at the three phase interface, which results in with significant electrostatic potential gradients extending a few nanometers into an—the insulating phase. This EDL spillover phenomenon is studied using scanning electrochemical cell microscopy to interrogate the oxidation of ferrocene in toluene to ferrocenium in water, $(Fc)_{tol} \rightarrow (Fc^+)_{aq} + e^-$, where $(Fc)_{tol}$ is simultaneously oxidized within ~ 1 nm of the toluene/ water/electrode interface and transferred into the aqueous phase to generate $(Fc^+)_{a\bar{q}}$. Finite element method simulations of provide insight on the electrostatic potential distribution and species concentration profiles in the proximity of the three phase interface and enable the calculation of complete *i-E* curves that incorporate for Fe CEPhT with inclusion of mass transport, electron transfer, phase transfer, and EDL structure. Simulated and experimental i-E traces show good agreement in the current magnitude and the effect of supporting electrolyte, demonstrating identifying an unexpected dependence of overall reaction kinetics on the concentration of supporting electrolyte in the aqueous phase due to EDL spillover. The presence of aAn interfacial toluene/water mixing region generates a unique electrochemical microenvironment where concerted electron transfer and solvent shell replacement facilitate CEPhT. Kinetic expressions for concerted and sequential CEPhT mechanisms are developed, highlighting the role of the this interfacial environment in controlling the rate of CEPhT. These combined experimental and simulated results are the first to support a concerted mechanism for CEPhT where (Fc)_{tol} is transported to the interfacial mixing region at the three-phase interface where it undergoes oxidation and phase transfer. EDL spillover can be leveraged for engineering sample geometries and electrostatic microenvironments to drive electrochemical reactivity in classically forbidden regions – , such ase.g-., insulating solvents and gases.

Keywords: Electrical double layer, Electron Transfer, Phase Transfer, Scanning Electrochemical Cell Microscopy, SECCM, Nanoelectrochemistry, Interfaces.

Introduction

Coupled electron- and phase-transfer (CEPhT) reactions are integral in numerous electrochemical systems such as the electrodeposition of metals from solvated metal ions, ^{1, 2} electrochemical amalgam formation,³ metal corrosion in mixed solvents, ^{4, 5} cation desolvation and intercalation in alkali-ion batteries, ^{6, 7} and multiphasic photocatalytic systems. ^{8, 9} These processes are typically accompanied by partial ¹⁰ or complete replacement of the local solvent environment. ¹¹ For example, during a simple electrodeposition process, such as the reduction of Cu²⁺ onto a Cu electrode, the metal ion undergoes several elementary reaction steps including: i) transport towards the electrode surface, ii) solvent shell reorganization/removal, iii) electron transfer to reduce the metal ion, and iv) phase transfer onto the metal electrode crystal lattice. Notably, CEPhT reactions can couple the electron and phase transfer elementary steps in a sequential or a concerted manner, with important consequences to their mechanism. Attempts to apply Marcus-type descriptions to these CEPhT systems are complicated by the extensive changes in the local chemical environment. ¹²⁻¹⁴ Furthermore, mixing over nanometer length-scales between two different phases results in a gradient of physical and chemical properties in the solvent medium. ¹¹ Fundamental kinetic and mechanistic insight of CEPhT reactions would benefit from the development of model systems where the electrochemical microenvironment can be precisely controlled and characterized.

Herein, we report an investigation of a model CEPhT system comprising the oxidation of ferrocene (Fc) to ferrocenium (Fc⁺) at a glassy carbon (GC)/toluene/water interface, represented by the overall reaction:

$$(Fc)_{tol} \to (Fc^+)_{aq} + e^-$$
 (Eq. 1)

where the subscripts "tol" and "aq" explicitly indicate that the electron-transfer (ET) step is accompanied by phase transfer (PhT) of the redox species from toluene to the aqueous phase. Experimentally, scanning electrochemical cell microscopy (SECCM) is used to form nanoscale three-phase interfaces – a nanopipette filled with an aqueous electrolyte is submerged into a bulk toluene phase containing Fc, and the toluene/water interfacial meniscus is brought in contact with an electrode surface, represented

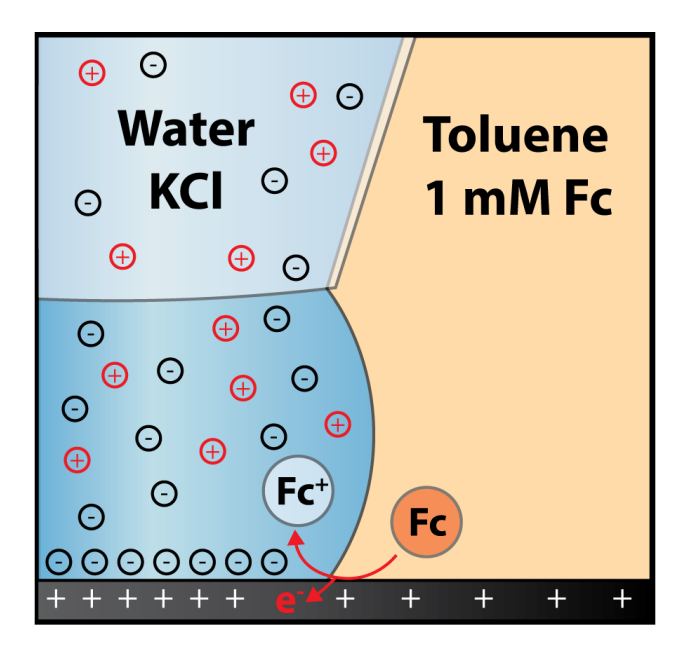


Figure 1. Experimental schematic of SECCM voltammetry for oxidative Fc CEPhT at the electrode/toluene/water (KCl) /electrode three-phase interface formed at the tip of a nanopipette filled with aqueous electrolyte and submerged in a bulk toluene phase

schematically in Figure 1. After the three-phase meniscus is formed, the oxidation of $(Fc)_{tol}$ to $(Fc^+)_{aq}$ can be driven by applying a potential to the glassy carbon (GC) electrode. Previously, we have studied the electrochemical CEPhT of Fc at wire electrodes across 1,2-dichloroethane (DCE, 100 mM TBAPF₆)/water (100 mM KCl) interfaces, ¹⁵ revealing a reversible *sequential* mechanism where the electron-transfer and phase-transfer steps occur separately. Subsequently, and to be detailed in a separate report, we experimentally investigated the case of *concerted* CEPhT using SECCM to study the oxidation of various Fc derivatives at the electrode/toluene/water interface. However, a mechanistic description of concerted CEPhT remains elusive because the role of the chemical microenvironment in these complex reactions is difficult to probe at the three-phase interface solely through experimental voltammetry.

Herein, we combine SECCM and finite element method (FEM) simulations to interrogate the role of the local electrochemical microenvironment at the three-phase boundary on the voltammetric response associated with CEPhT. First, we report the oxidation of Fc across the toluene/water interface using SECCM voltammetry, demonstrating a concerted CEPhT mechanism. FEM simulations are developed to describe the complete *i-E* response associated with CEPhT, with explicit treatment of mass transport,

electron- and phase-transfer kinetics, the electrostatic potential distribution (including the EDL), and the presence of an interfacial water/toluene mixing region. This model reveals that EDL spillover into the toluene phase – extending a few nanometers into the toluene phase – provides the driving force for the net reaction. This driving force is sensitive to the EDL structure, and simulations predict a reduction of the overall reaction kinetics upon lowering the concentration of supporting electrolyte in the aqueous phase. This prediction is tested experimentally using SECCM, demonstrating good agreement between simulated and experimental *i-E* responses under varying electrolyte concentrations. This combined experimental and simulation effort provides the theoretical framework to understand concerted CEPhT reactions and to inform the design of new electrochemical systems taking advantage of EDL spillover to drive unexpected reactivity. Finally, experimental and numerical results are complemented by an analytical treatment of the system, where kinetic expressions that account for the elementary steps of electron- and phase-transfer are developed.

Results and Discussion

Experimentally Observing Concerted CEPhT Using SECCM

SECCM voltammetry was used to probe the mechanism of concerted Fc oxidative CEPhT at electrode/toluene/water (KCl) three-phase interfaces, as represented schematically in Figure 1. Briefly, a laser-pulled nanopipette (tip radius ~150-300 nm) is filled with an aqueous electrolyte containing KCl, forming a hanging aqueous meniscus at the nanopipette tip. ¹⁶ To enable electrochemical characterization of the electrode/aqueous electrolyte interface, 0.5 mM Ru(NH₃)₆Cl₃ is added to the aqueous phase; however, this species is not involved in the CEPhT mechanism. A Ag/AgCl wire is inserted into the pipette to act as a combined counter/reference electrode for voltammetric measurements. The nanopipette and hanging aqueous meniscus are lowered under three-dimensional piezoelectric control towards a GC electrode that is submerged in a bulk toluene phase and polarized at a potential sufficient to reduce Ru(NH₃)₆³⁺. When the droplet comes into contact with the GC electrode, a faradaic current associated with Ru(NH₃)₆³⁺ reduction is observed, and the piezoelectric translation is stopped. The resultant

electrode/toluene/water three-phase electrochemical cell is stable under repeated voltammetric cycling, as evidenced by a consistent Ru(NH₃)₆³⁺ voltammetric wave (see SI Section II). These stable electrochemical cells provide a method to directly and rapidly probe the current associated with CEPhT processes at the electrode/toluene/water three-phase interface, such as Fc oxidation.

The cyclic voltammetric response for a pipette containing an aqueous phase of 100 mM KCl and 0.5 mM Ru(NH₃)₆Cl₃ in contact with a GC electrode submerged in pure toluene is shown by the black trace in Figure 2. The response shows only a voltammetric wave associated with Ru(NH₃)₆³⁺ reduction in the aqueous phase and no voltammetric features at positive potentials. We note that the capacitive background in all voltammetric scans is several orders of magnitude too large to arise from double layer charging, and is attributed to stray capacitance in the SECCM instrument. Subsequently, the bulk toluene phase was replaced with toluene containing 1 mM Fc and the cyclic voltammetry was repeated, as shown by the red trace in Figure 2. Importantly, the voltammetric wave for Ru(NH₃)₆³⁺ reduction remains largely unchanged with bulk phase replacement, indicating a stable meniscus geometry and reproducible positioning of the SECCM tip. In the presence of Fc, a new oxidative voltammetric feature is observed

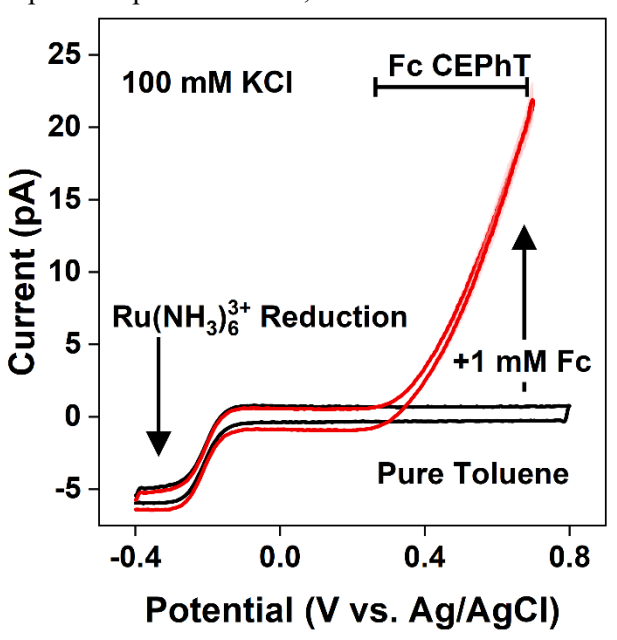


Figure 2. Experimental voltammetry for nanopipettes containing water with 0.5 mM Ru(NH₃)₆Cl₃ and 100 mM KCl submerged in either pure toluene (black) or toluene containing 1 mM Fc (red). In the presence of Fc, an oxidative wave associated with Fc CEPhT is observed around 0.25 V versus Ag/AgCl. The nanopipette radius is \sim 250 nm and the voltametric scan rate is 50 mV/s.

with an onset around +250 mV versus Ag/AgCl (100 mM Cl⁻). While the voltammetric wave for Ru(NH₃)₆³⁺ reduction is marked by a sharp sigmoidal *i-E* profile due to fast electron transfer kinetics that allow it to rapidly reach its mass transport limit, the slow exponential rise in the *i-E* profile for Fc oxidation suggests a kinetically controlled reaction. The voltammograms correspond to the average of nine isolated SECCM meniscus cells where the standard deviation of the current for nine measurements is approximately the width of the lines, indicating excellent reproducibility in the observed CEPhT response. While the new voltammetric wave in Figure 2 can be unequivocally assigned to Fc oxidation at the three-phase interface, the role of the electrochemical microenvironment in governing CEPhT activity has not been investigated.

Model Expressions for Concerted CEPhT

A schematic of the three-phase interface and the associated CEPhT reaction are shown in Figure 3. As described in detail below, we model the interface between toluene and water as a mixed layer of \sim 1 nm width. Within this toluene/water mixing region at the electrode surface, concerted CEPhT proceeds by the oxidation and phase transfer of $(Fc)_{tol}$ to $(Fc^+)_{aq}$, indicated by (i) in Figure 3. For the simple concerted mechanism, a Butler-Volmer type rate expression can be written as:

$$\frac{d}{dt} \left(C_{\text{Fc}}^{\text{T}} \right) = -\frac{d}{dt} \left(C_{\text{Fc}^+}^{\text{W}} \right) = k_{\text{CEPhT}}^0 \cdot \left[C_{\text{Fc}^+}^{\text{W}} \, \mathrm{e}^{-\alpha f \eta} \, - C_{\text{Fc}}^{\text{T}} \, \mathrm{e}^{(1-\alpha)f \eta} \right] \ (\text{Eq. 2})$$

where C_{Fc}^{T} is the concentration of Fc in the toluene phase, C_{Fc}^{W} is the concentration of Fc⁺ in the aqueous phase, k_{CEPhT}^0 is the CEPhT rate constant, α is the transfer coefficient, f = F/RT is the reduced Faraday's constant, and the overpotential $\eta = (\phi_M - \phi_{\text{PET}} - E^0)$ is the difference between the electrode potential ϕ_M , the potential at the plane of electron transfer, ϕ_{PET} , and the formal redox potential for Eq. 1, E^0 . Eq. 2 contains two subtle but key differences from the standard Butler-Volmer (BV) model expressions. First, in the reduced and oxidized forms of the redox species, i.e., Fc and Fc⁺, are located in different phases. Thus, Eq. 2 represents a BV expression for a concerted electron- and phase-transfer process, where E^0 is determined by the free energies of Fc in toluene and Fc⁺ in water. As E^0 , k^0 , and α in Eq. 2

are defined with respect to the CEPhT reaction coordinate, it is important to note that these values are distinct from those corresponding to an electron-transfer step in either pure phase. Second, and as detailed below, $\phi_{\rm PET}$, and, thus, the driving for electron transfer, is a function of position along the GC electrode as one moves across the water/toluene interface. As the electron- and phase-transfer steps are implicitly connected in CEPhT reactions, the value of $k_{\rm CEPhT}^0$ is governed by descriptors for both molecular processes.

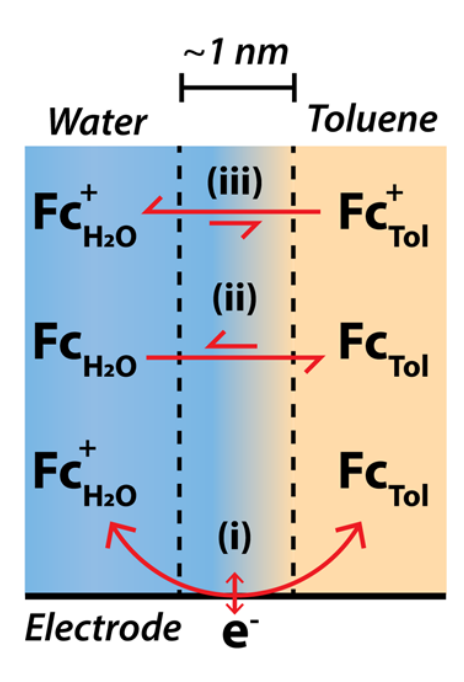


Figure 3. Schematic representation of processes during Fc oxidative CEPhT including (i) concerted electron- and phase-transfer at the electrode/toluene/water three-phase interface, (ii) Fc partitioning at the water/toluene interface, and (iii) Fc⁺ partitioning at the water/toluene interface. All processes include transfer across the toluene/water mixing region with accompanying implicit solvent shell replacement.

At the liquid/liquid phase boundary extending beyond the three-phase interface, conventional phase transfer for Fc and Fc⁺ are indicated by (ii) and (iii) in Figure 3, respectively. The corresponding rate expressions for phase transfer can be written as:

$$\frac{d}{dt}\left(C_{Fc}^{T}\right) = -\frac{d}{dt}\left(C_{Fc}^{W}\right) = k_{PT,Fc} \left(K_{Fc}^{eq} C_{Fc}^{W} - C_{Fc}^{T}\right)$$
 (Eq. 3a)

$$\frac{d}{dt}(C_{Fc^{+}}^{T}) = -\frac{d}{dt}(C_{Fc^{+}}^{W}) = k_{PT,Fc^{+}}(K_{Fc^{+}}^{eq}C_{Fc^{+}}^{W} - C_{Fc^{+}}^{T})$$
 (Eq. 3b)

where $k_{\rm PT,i}$ is the phase transfer rate constant for species i, and $K_{\rm i}^{eq}$ is the phase transfer equilibrium constant for species i, defined as $K_{\rm i}^{eq} = C_{\rm i}^{\rm T}/C_{\rm i}^{\rm W}$. The phase transfer processes at the toluene/water boundary of the SECCM meniscus can be simplified by considering the high value of $K_{\rm FC}^{eq}$ due to the negligible solubility of Fc in the aqueous phase (~40 μ M).¹⁷ Thus, the rate of Fc phase transfer, Eq. 3a, is approximately zero, and only the kinetics of the CEPhT process (Eq. 2) and the partitioning of Fc⁺ (Eq. 3b) contribute to the observed i-E response.

To simulate the overall Fc CEPhT reaction at the electrode/toluene/water interface, the kinetic expressions in Eqs. 2-3 must be combined with treatments of mass transport, the electrostatic potential distribution including the EDL, and the structure of the water/toluene interface. Molecular transport for Fc/Fc⁺ in both phases and supporting electrolyte in the aqueous phase was described by the Nernst-Planck¹⁸ equation:

$$J_i = -D_i \nabla C_i - z_i f D_i C_i \nabla \phi \tag{Eq. 4}$$

where subindex i enumerates all molecular/ionic species whose molecular flux J_i , depends on their diffusion coefficient D_i , their concentration C_i , and their charge z_i . ∇ is the gradient operator, ϕ is the electrostatic potential, F is Faraday's constant, R is the gas constant, and T is the temperature. The electrostatic potential distribution in the aqueous phase is computed from the Poisson equation, given by:

$$\nabla^2 \phi = -\frac{F \sum z_i C_i}{\varepsilon \varepsilon_0}$$
 (Eq. 5)

where ε_0 is the permittivity of free space, ε is the relative permittivity of bulk water (~78), and all other variables have been previously described. The EDL at the electrode/water (KCl) interface was treated using the Bockris-Devanathan-Müller model with explicit inner and outer Helmholtz layers. ¹⁹ The inner Helmholtz plane (IHP), corresponding to the plane of closest approach for desolvated ions, was set at a distance of 0.29 nm and the dielectric constant between the electrode surface and the IHP was set at 6. ²⁰ The outer Helmholz plane (OHP), corresponding to the plane of closest approach for solvated ions, was set at a distance of 0.59 nm and the dielectric constant between the IHP and OHP was set at 30. As the

compact EDL in the aqueous phase is impermeable to ions, the electrostatic potential distribution is given by the Laplace equation,

$$\nabla^2 \phi = 0 \tag{Eq. 6}$$

and the surface charge density at the outer Helmholtz plane (OHP), σ_{OHP} , is defined as:

$$\sigma_{\text{OHP}} = -\varepsilon \varepsilon_0 \nabla \phi|_{\mathbf{x} = \text{OHP}}.\tag{Eq. 7}$$

As no electrolyte ions are present in the toluene phase, the electrostatic potential distribution at all points in the toluene phase is given by the Laplace equation, Eq. 6.

To treat the interfacial structure of the water/toluene boundary, this model includes the presence of a mixing region extending ± 0.5 nm from the nominal liquid/liquid boundary, based on insight from molecular dynamics simulations. Over this interfacial mixing region, the distance-dependent chemical composition was approximated as a smoothed Heaviside function as:

$$\chi_{H_20}(x) = \begin{cases} 1 & \text{if } x \le -\delta \\ 0.5 - 0.75 \left(\frac{x}{\delta}\right) + 0.25 \left(\frac{x}{\delta}\right)^3 & \text{if } -\delta < x < \delta \\ 0 & \text{if } x \ge \delta \end{cases}$$
 (Eq. 8)

where x is the distance relative to the nominal three-phase interface and 2δ is the thickness of the mixing region, here set to $\delta = 0.5$ nm. The molar fraction of toluene is the complement, $\chi_{Tol}(x) = 1 - \chi_{H_2O}(x)$. The chemical composition and distance-dependent dielectric constant calculated from mole fractions²¹ as:

$$\varepsilon(x) = \chi_{H_2O}(x)\varepsilon_{H_2O} + \chi_{Tol}(x)\varepsilon_{Tol}$$
 (Eq. 9)

are shown in Figure 4. In the absence of experimentally measured dielectric constants at the water/toluene interface, the dielectric constant in the mixing region was approximated using a linear model. Ions from the supporting electrolyte are allowed to diffuse in the aqueous side of this interface (x < 0). Within the interfacial region, and extending an additional 1.5 nm into the pure toluene phase, both(Fc)_{tol} and (Fc⁺)_{aq} were permitted to diffuse and undergo the concerted CEPhT reaction – an approximation required for mass conservation in the overall CEPhT reaction. Within the mixing region, mass transport

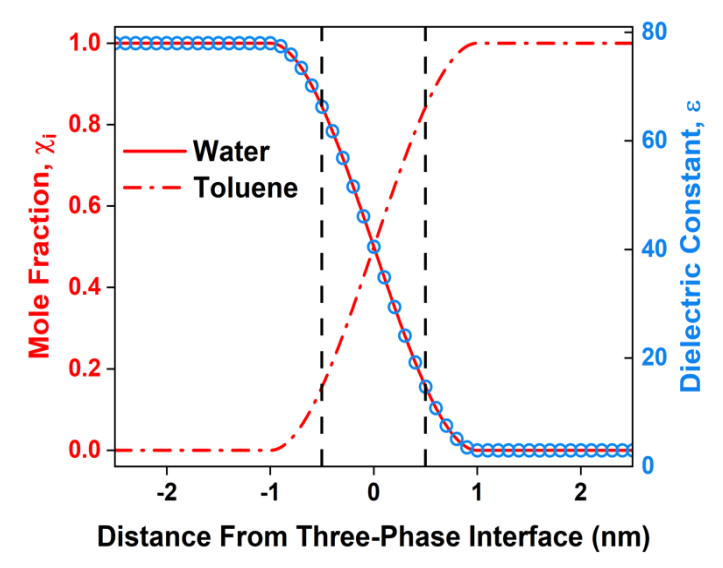


Figure 4. Solvent composition (left, red lines) and dielectric constant (right, blue points) near three-phase interface, with mixing region extending ± 0.5 nm beyond the nominal three-phase interface indicated by dashed black lines.

for $(Fc)_{tol}$ and $(Fc^+)_{aq}$ were defined identically to transport within the bulk phases. The distance of 1.5 nm was selected based on the distance over which the electrochemical driving force for CEPhT dissipates in the toluene phase (*vide infra*). However, this approximation does not alter the physical interpretation of the concerted CEPhT process due to: i) the rapid transport of $(Fc^+)_{aq}$ away from the three-phase interface and into the bulk aqueous phase after CEPhT and ii) the fact that the CEPhT reaction takes place at a sufficiently high positive electrode potential such that the reduction of $(Fc^+)_{aq}$ to $(Fc)_{tol}$ is negligible in the mixing region and in the bulk toluene phase.

Simulation of Fc CEPhT at the GC/Toluene/Water Interface

Finite element model simulations of the oxidation of Fc at the GC/toluene/water three-phase boundary in the SECCM configuration were implemented with COMSOL Multiphysics V5.5 by combining Eqs. 2-9 with appropriate bulk solution and electrostatic boundary conditions, detailed fully with the simulated geometry in SI Section III (Figure S6). From these simulations, the *i-E* response, the electrostatic potential distribution, and concentration distributions can be analyzed to understand the role

of the electrochemical microenvironment on CEPhT reactivity. Complete simulation details are provided in the COMSOL model report provided in the supporting information.

A simulated electrostatic potential profile for the case of 100 mM KCl and $\phi_{\rm M} = 0.8$ V versus pzc (potential of zero charge) is shown in Figure 5A within 150x150 nm of the three-phase interface. In the aqueous meniscus phase, the electrostatic potential drops across the EDL to ~0 V versus pzc at the OHP. At the other extreme, consider the toluene phase at distances far away from the three-phase interface, where the absence of supporting electrolyte ions results in a linear potential drop between the electrode surface and ground, here corresponding to the bulk solution boundary. The lack of a toluene-phase EDL and the large separation between the electrode and ground establishes a small electrostatic potential gradient in toluene, which results in insufficient driving force for Fc oxidation, $\eta = (\phi_M - \phi_{PET} E^0$) ~ 0. However, near the GC/toluene/water interface, the electrostatic potential gradient between the electrode surface and the PET begins to increase appreciably. The electrostatic potential profile within a 10x10 nm region at the three-phase interface is shown on the right in Figure 5B, revealing that the potential drop across the aqueous phase diffuse EDL results in a noticeable electrostatic potential gradient in the toluene region near the three-phase interface. This potential gradient in the toluene region near the three-phase interface – the EDL spillover effect – provides sufficient driving force for Fc oxidation within the insulating toluene phase, with a contribution that diminishes rapidly as a function of distance away from the three-phase interface.

The corresponding Fc concentration profile at the three-phase interface is shown in Figure 5C, demonstrating the depletion of Fc within a few nm of the three-phase interface. Conversely, the concentration profile for Fc⁺, shown in Figure 5D, reveals significant Fc⁺ accumulation *within* the aqueous phase droplet approaching ~3 mM, due to the high rate of CEPhT. Fc⁺ in the aqueous phase is transported by diffusion and migration away from the three-phase interface into the bulk aqueous phase in the nanopipette, and the bulk concentration at distances far from the electrode/electrolyte interface approaches 0 mM (Figure S7). The concentration profiles for Fc and Fc⁺ along the PET are shown in Figure 5E.

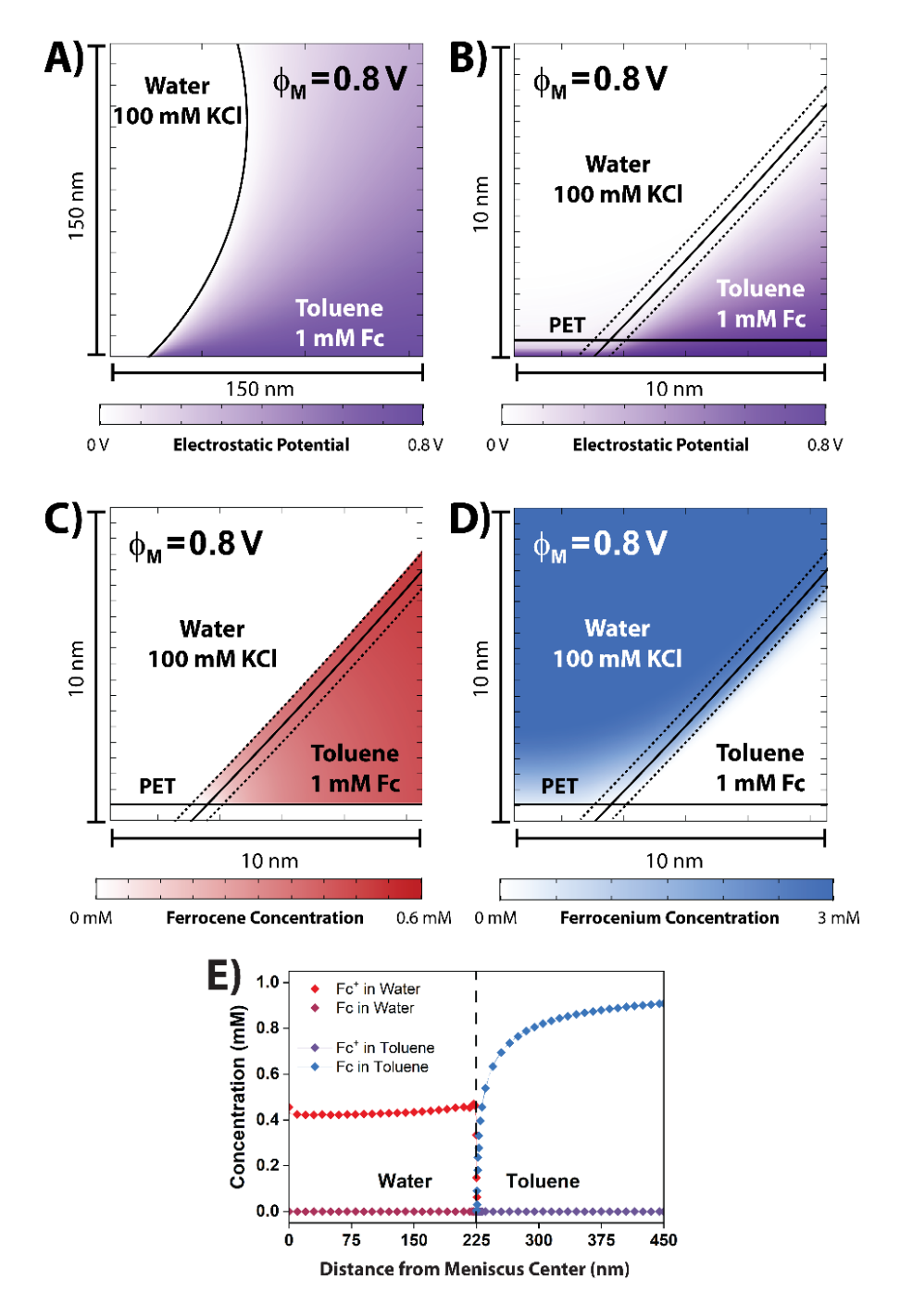


Figure 5. Electrochemical microenvironment near the three-phase interface at 100 mM supporting electrolyte. A) Simulated electrostatic potential profile within 150x150 nm of the three-phase interface for an aqueous phase containing 100 mM KCl. B) Electrostatic potential profile within a 10x10 nm region of the three-phase interface showing EDL spillover into toluene phase. C) Fc concentration profile corresponding to B, demonstrating Fc depletion in toluene phase directly at the three-phase. D) Fc⁺ concentration profile as in C. All simulations correspond to a nanopipette radius of 225 nm, 1 mM Fc in the toluene phase, $\theta = 45^{\circ}$, $k_{PT} = 10$ cm/s, and $k_{CEPhT}^{0} = 0.1$ cm/s. The mixing region is indicated by the dashed black lines, and the nominal toluene/water boundary is indicated by the solid black line. E) Concentration profiles along the plane of electron transfer for Fc and Fc⁺. The three-phase interface is located at R=225 nm, denoted by the vertical dotted line, with the water region at r<R and toluene for

To quantitatively probe the effect of EDL spillover on Fc CEPhT, we now consider the electrochemical driving force near the three-p hase interface as a function of applied electrode potential. Figure 6A shows the potential drop at the PET, $(\phi_{\text{M}}-\phi_{\text{PET}})$, as a function of distance along the electrode surface at a range of applied electrode potentials, with the three-phase interface indicated by the dashed line. In the aqueous phase (left), the rapid electrostatic potential drop across the compact EDL results in $(\phi_{\rm M}-\phi_{\rm PET})$ that is approximately equal to the applied potential. Due to the lack of ions in the toluene phase, $(\phi_{\text{M}}-\phi_{\text{PET}})$ is ~ 0 V within tens of nm of the three-phase interface at all applied potentials (right). The potential drop from Figure 6A is shown in Figure 6B within ±5 nm of the three-phase interface, demonstrating the rapid drop in $(\phi_{M}-\phi_{PET})$ along the electrode surface in the insulating organic phase. The toluene/water mixing region is represented by the vertical dashed red lines, with a thickness of 1 nm. This location-dependent driving force (ϕ_{M} - ϕ_{PET}) predicts that the rate of Fc oxidation at the electrode/organic interface will rapidly decrease as the distance from the three-phase interface increases. Figure 6C shows the simulated current density for Fc oxidation in the mixing region and in the toluene phase as a function of distance from the three-phase interface at a range of applied electrode potentials. As the applied potential is increased from 0.4 V, the current density distribution increases in the mixing region and ultimately shifts towards the toluene phase up to 0.8 V, consistent with the increased effective driving force shown in Figure 6B. At all simulated potentials for this meniscus geometry, electron-transfer in the toluene phase is restricted to within 1 nm of the nominal three-phase interface, occurring primarily within the toluene/water mixing region.²² The spatial confinement of the CEPhT to length-scales associated with the thickness of the interfacial solvent region is physically consistent with a concerted CEPhT mechanism. As Fc is insoluble in the aqueous phase, the simulated current density beyond the mixing region into the aqueous phase is zero.

To understand the role of the electrical double layer on CEPhT, the voltammetric response for Fc oxidation at the SECCM electrode/toluene/water interface was simulated as a function of supporting electrolyte concentration. Qualitatively, as the concentration of supporting electrolyte is decreased, a

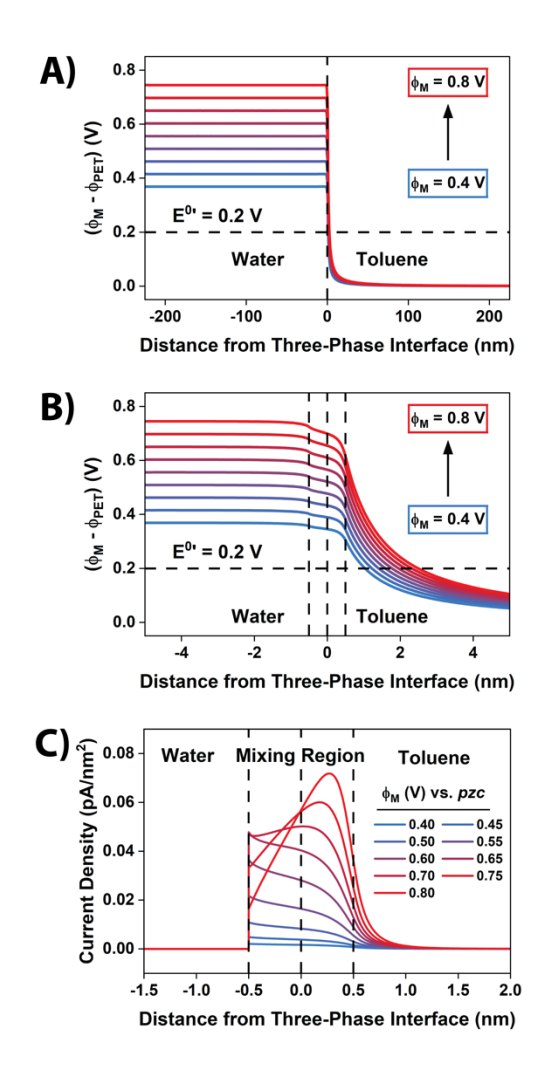


Figure 6. Electrostatic potential drop and current density at the three-phase interface. A) Potential drop at the PET, $(\phi_{\rm M} - \phi_{\rm PET})$, as a function of distance from the three-phase interface at a range of electrode potentials, $\phi_{\rm M}$, for a nanopipette containing 100 mM KCl. B) Potential drop at the PET, as in A, within ±5 nm of the three-phase interface. C) Current density for Fc oxidative CEPhT as a function of distance from the three-phase interface extending into the toluene phase at a range of electrode potentials. All simulations correspond to a nanopipette radius of 225 nm, 1 mM Fc in the toluene phase, $\theta = 45^{\circ}$, $k_{\rm PT} = 10$ cm/s, and $k_{\rm CEPhT}^0 = 0.1$ cm/s. The mixing region boundaries are indicated by the red dashed vertical lines.

inspection of Figure 6, the driving force for CEPhT is clearly related to the potential ϕ_{PET} , implicating the electrolyte concentration on resultant current-voltage behavior for Fc oxidation. A set of simulated voltammograms for a 225 nm radius nanopipette containing 1 mM to 200 mM KCl supporting electrolyte, submerged in a toluene phase containing 1 mM Fc, is shown in Figure 7A, demonstrating a cathodic shift in the Fc CEPhT wave with increasing concentrations of supporting electrolyte. The predicted effect of

supporting electrolyte concentration on the apparent kinetics of the Fc CEPhT process was tested experimentally using SECCM, as discussed above for Figure 2. Importantly, as the nanopipette laser-pulling process generates a pair of "twin" nanopipettes with nominally identical radii, the effect of aqueous supporting electrolyte concentration on Fc CEPhT can be directly probed by comparing the voltammetric response of twin nanopipettes. Discussion of nanopipette characterization and a comparison of "twin" pipettes containing the same aqueous electrolyte composition are reported in SI Section II.

A set of cyclic voltammograms for the oxidation of 1 mM Fc at the GC/toluene/aqueous electrolyte three-phase interface is shown in Figure 7B for a pair of nanopipettes containing 0.5 mM Ru(NH₃)₆³⁺ and either 0 mM (blue) or 100 mM (red) additional KCl supporting electrolyte. Figure 7B reveals a significant cathodic shift in the voltammetric response for Fc CEPhT in the presence of 100 mM KCl, consistent with the simulated response. The slightly increased current associated with Ru(NH₃)₆³⁺ reduction in the absence of excess supporting electrolyte is consistent with migration effects previously reported.²³ The order of magnitude agreement in the simulated and experimental currents for Fc CEPhT allow us to obtain insight on the driving force and operative parameters for concerted CEPhT. The simulated voltammetry in Figure 7 is presented relative to the pzc of glassy carbon, which has been previously reported at ~100 mV versus Ag/AgCl. While we do not explicitly measure this value for our experimental system, the net effect of assuming a pzc of +100 mV versus Ag/AgCl is an anodic shift in the simulated voltammetric waves by approximately 100 mV. Quantitative fitting of these voltammetric responses is beyond the scope of this work, requiring full characterization of the pzc at the nanoscale three-phase cell, the interfacial meniscus geometry under electric fields, electron- and phase-transfer rate constants, and the role of solvent shell replacement during CEPhT. However, simulated voltammograms are presented in SI Section VI, demonstrating that changing the nanopipette radius, meniscus geometry, transfer coefficient, and CEPhT rate constant do not alter our interpretation of the resultant CEPhT voltammetry.

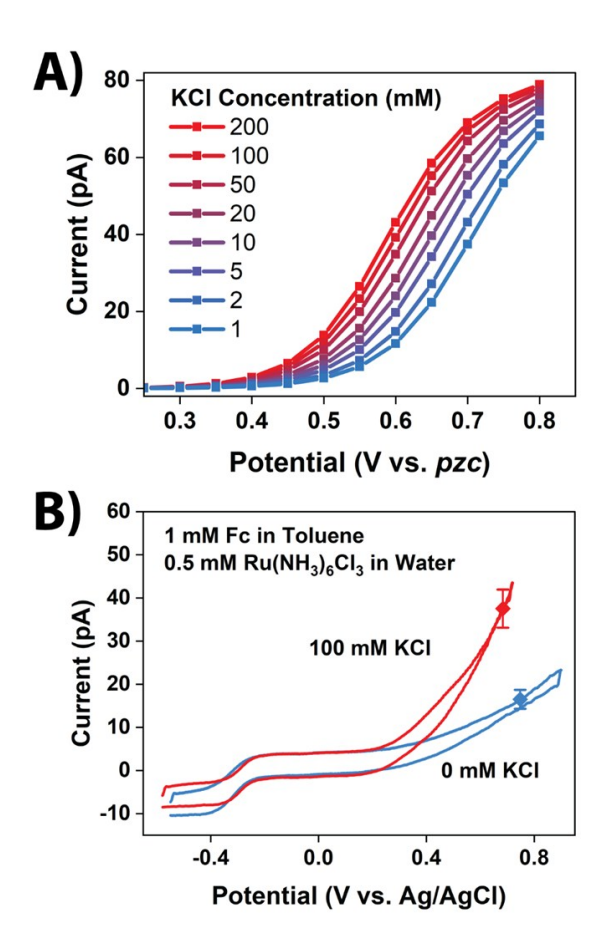


Figure 7. A) Simulated *i-E* response for the oxidative CEPhT Fc at the electrode/toluene/water three-phase interface as a function of supporting electrolyte concentration, predicting cathodic shift in voltammetric profile with increasing electrolyte concentrations. Simulations correspond to a nanopipette radius of 225 nm, 1 mM Fc in the toluene phase, $\theta = 45^{\circ}$, $k_{\text{PT}} = 10 \text{ cm/s}$, and $k_{\text{CEPhT}}^0 = 0.1 \text{ cm/s}$. B) Experimental three-phase SECCM voltammetry for 1 mM Fc CEPhT with excess supporting electrolyte of 100 mM KCl (red) or 0 mM KCl (blue), demonstrating cathodic shift in voltammetric profile with increasing electrolyte concentration, as predicted in A. For the experimental voltammetry, the nanopipette radius is ~250 nm and the voltametric scan rate is 50 mV/s.

Mechanism of Fc CEPhT at the GC/Toluene/Water Interface

Within the previous sections, we have modeled the oxidative CEPhT of Fc assuming a concerted mechanism, where the electron- and phase-transfer steps occur simultaneously at the three-phase interface, indicated by (i) in Figure 8. However, an alternative mechanism comprising sequential electron- and phase-transfer steps may be more appropriate when considering solvation dynamics at the three-phase boundary, analogous to a square-scheme in proton-coupled electron transfer reactions. Classical electron-transfer processes are accompanied by a reorganization of the solvation shell, changing with the

perturbation of bond lengths within the redox species, indicated by solvent motion during the ET steps in Figure 8. A molecule partitioning between liquid phases experiences a full replacement of the solvent shell as it traverses the liquid/liquid mixing region, shown in the PhT steps in Figure 8. For a sequential CEPhT mechanism, the reaction can proceed through an initial ET step followed by a PhT step (ii, ET-PhT) or an initial PhT step followed by an ET step (iii, PhT-ET). At this stage, we cannot determine whether Fc partially desolvates and chemisorbs to the GC electrode to undergo ET, or if electron transfer occurs with Fc in the solution phase in a Marcus type process. However, analyzing the kinetics of sequential CEPhT mechanisms may provide insight on the relative contributions of the ET and PhT steps in controlling overall reactivity.

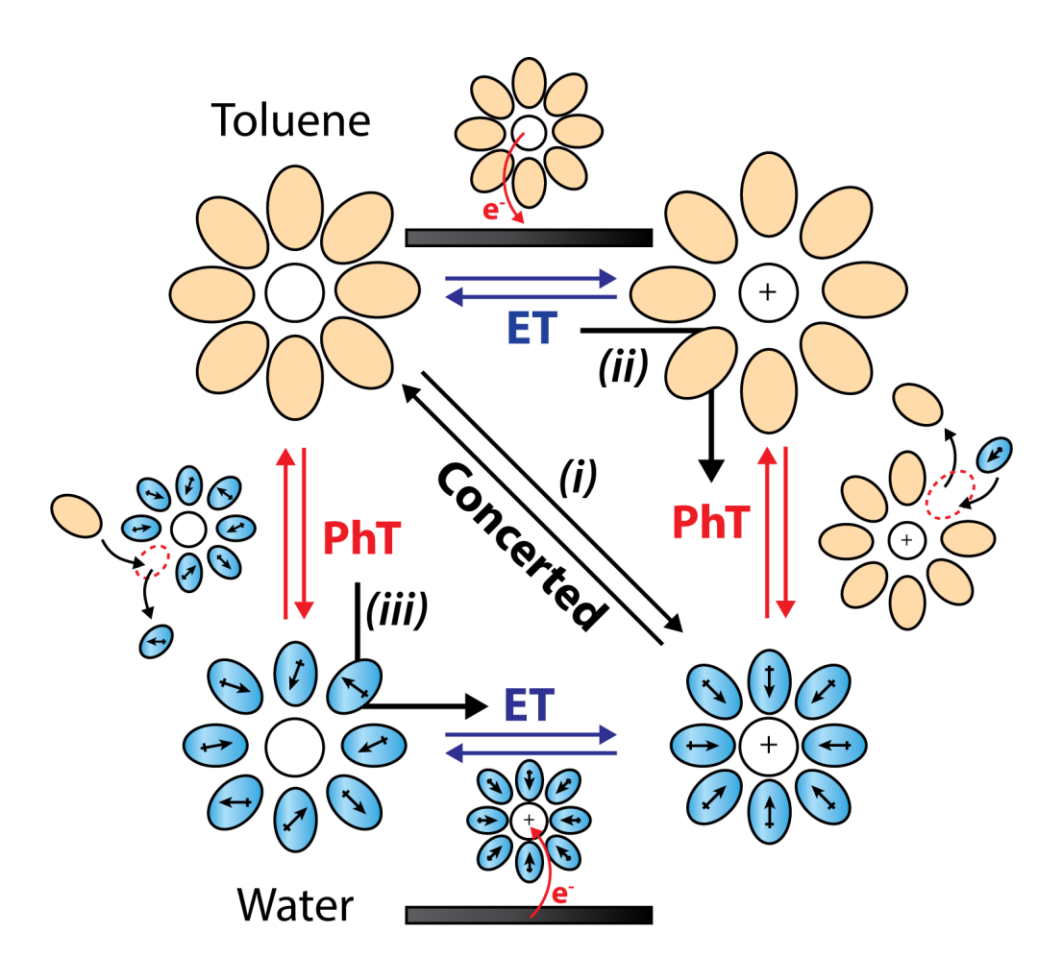


Figure 8. CEPhT reaction square scheme demonstrating the behavior of the solvation shell during electron-transfer (blue) and phase-transfer (red) steps at the three-phase electrode/toluene/water interface. The oxidation of Fc_{Tol} to Fc_{H2O}^+ can follow a concerted (i), ET-PhT (ii), or PhT-ET (iii) mechanism.

The above FEM simulations provide a sound foundation to disentangle the CEPhT mechanism into elementary ET and PhT steps. In light of the observation of a significant EDL spillover into the toluene phase and the resulting current density beyond the nominal water/toluene interface, we consider the kinetics of the ET-PhT sequential mechanism where Fc is oxidized to Fc⁺ in the toluene phase and subsequently transfer across the toluene/water boundary to yield Fc⁺ in water. In this analytical treatment, the mixing region is not explicitly included. Instead, we consider a sharp nominal interface where the PhT step occurs —the sequential replacement of individual solvent molecules in the solvation shell as Fc traverses the toluene/water mixing region is beyond the scope of this present work. Finally, analogous to the concerted CEPhT mechanism, we assume that the rate of Fc partitioning across the toluene/water interface is approximately zero due to the low solubility of Fc in water. In summary, we described the overall CEPhT reaction in this SECCM experiment as

$$(Fc)_{tol} \overset{k_{ox}}{\underset{k_{red}}{\longleftarrow}} (Fc^{+})_{tol} \overset{k_{PT}}{\underset{k'_{PT}}{\longleftarrow}} (Fc^{+})_{aq}$$
 (Eq. 10)

where the ET step takes place in the toluene phase and follows standard Butler-Volmer kinetics ($k_{ox} = k_{ET} \cdot e^{(1-\alpha)f\eta}$, $k_{red} = k_{ET} \cdot e^{-\alpha f\eta}$) and the phase transfer rates reflect the equilibrium of Fc⁺ concentrations in the bulk toluene and water phases, $k_{PT}/k'_{PT} = K^{eq}_{Fc^+} = C^T_{Fc^+}(\infty)/C^W_{Fc^+}(\infty)$ – with the caveat that we are considering $C^W_{Fc^+}(\infty)$ to be the concentration of Fc⁺ in the core of the meniscus. Finally, this section is concerned with the steady state properties of the system, which are reflected in the *i-E* voltammograms, but does not include their transient behavior.

To disentangle the elementary electron transfer (ET) and phase transfer (PhT) steps, we developed an analytical treatment of the flux of molecules undergoing oxidation/reduction reactions with the electrode (j_{ET}) and the phase transfer along the meniscus water/toluene interface (j_{PhT}). Because supporting electrolyte ions are not soluble in toluene, any *measured current* in SECCM experiments must be the result of a reaction that couples electron transfer and phase transfer, taking a neutral Fc in toluene to an oxidized Fc⁺ in water. This consideration requires the total PhT flux to equal the total ET flux

$$\oint_{PET} j_{ET} d\Omega_{PET} = \oint_{A} j_{PhT} d\Omega_{A}$$
 (Eq. 10)

noting that the ET flux is integrated over the plane of electron transfer (PET) and the PhT flux is integrated over the water/toluene interface (i.e., the surface of the SECCM meniscus). These fluxes are written as

$$j_{\text{ET}} = k_{\text{ET}} \cdot \left[C_{\text{Fc}}^{\text{T}}(\vec{r}) e^{(1-\alpha)f\eta(\vec{r})} - C_{\text{Fc}}^{\text{T}}(\vec{r}) e^{-\alpha f\eta(\vec{r})} \right]$$
 (Eq. 11a)

$$j_{\text{PhT}} = k_{\text{PhT}} \cdot \left[C_{\text{Fc}^+}^{\text{T}}(\vec{r}) - K_{\text{Fc}^+}^{eq} \cdot C_{\text{Fc}^+}^{\text{W}}(\vec{r}) \right]$$
 (Eq. 11b)

where the spatial dependence of the overpotential and Fc/Fc⁺ concentrations are explicitly noted. To simplify notation, we use spherical coordinates with an origin at the intersection of the PET and the symmetry axis of the nanopipette, and the equatorial plane coinciding with the PET, so the three-phase interface is located at coordinates r = R, $\theta = \frac{\pi}{2}$, $\varphi \in [0,2\pi]$.

A limited set of assumptions – grounded in experimental observables and/or numerical simulations – is sufficient to describe the ET-PhT process:

- (1) Because the EDL spillover effect is localized near the three-phase interface, the driving force for Fc oxidation within the toluene phase decays rapidly as r > R grows. The absence of current in the bulk toluene phase (away from the three-phase interface) implies that Fc/Fc⁺ must be at Nernstian equilibrium dictated by the potential in this region of the PET the lack of an EDL in the toluene phase away from the three-phase interface means the potential drop at the PET is minimal and $\eta \approx -E^0$. Inclusion of this equilibrium in an analytical expression for $j_{\rm ET}$ ensures convergence of the integral in Eq. 10.
- (2) Mass transport to and away from the interface is not treated explicitly; the steady-state concentration profiles of Fc/Fc⁺ are based on FEM simulation outcomes.
 - In water, the Fc⁺ concentration reaches equilibrium inside the meniscus rapidly. Similar to the FEM section above, Fc solubility in water is approximated as zero, and only the phase transfer of Fc⁺ is considered.

• In toluene, the concentration of Fc decreases from its bulk value $C_{Fc}^{T}(\infty)$ to a value at the interface $C_{Fc}^{T}(R)$; this depletion of Fc is bias-dependent and we represent it with a monotonic, smooth function $C_{Fc}^{T}(r) = C_{Fc}^{T}(R)h(r) + C_{Fc}^{T}(\infty)[1 - h(r)]$. With h(R) = 1 and $h(\infty) = 0$. Finally, the concentration of Fc⁺ in toluene is only allowed to deviate from its Nernstian equilibrium with a sharp spike at the interface, $C_{Fc}^{T}(r) = C_{Fc}^{T}(\infty) + C_{Fc}^{\Phi}(r-R)\delta\left(\theta - \frac{\pi}{2}\right)$, where the Dirac delta functions localize this spike at the intersection of the meniscus and the PET. In essence, Fc⁺ does not accumulate in bulk toluene – it is generated at the interface where the driving force for phase transfer is large.

It is thus possible to compute the integrals in Eqs. 10-11 (details in SI Section VII) and arrive at an expression for the SECCM current

$$\frac{i}{nF} \approx \left[\frac{2\pi k_{ET} k_{PhT} \xi_{EDL}}{k_{PT} + k_{ET} e^{-\alpha f} (\eta_{\phi} - E^0)} \cdot e^{-(1-\alpha)fE^0} \right] \cdot C_{Fc}^{T}(\infty)$$
 (Eq. 12)

where the term in brackets is the overall CEPhT rate k_{CEPhT} , and ξ_{EDL} is a scaling variable that represents the effect of EDL spillover and is determined by the spatially-dependent voltage drop at the PET, $\eta'(r) = \phi_M - \phi_{PET}(r)$, whose value at the interface η_{ϕ} is set by the EDL in the meniscus.

$$\xi_{EDL} = \int_{R}^{\infty} d\mathbf{r} \ r \, e^{-\alpha f \eta \prime (r)} \cdot \left\{ e^{f \eta \prime (r)} \cdot \left[1 + h(r) \cdot \left(\frac{C_{Fc}^{T}(R)}{C_{Fc}^{T}(\infty)} - 1 \right) \right] - 1 \right\}$$
 (Eq. 13)

It is informative to consider the limiting cases for Eq. 12. As expected, if ET and PhT are both prohibitively slow, such that $k_{ET}\approx 0$ and $k_{PhT}\approx 0$, the overall CEPhT rate approaches zero. If the phase transfer rate is much slower than the electron transfer rate, then $k_{CEPhT}\approx 2\pi k_{PhT}\xi_{EDL}\mathrm{e}^{-fE^0}\mathrm{e}^{\alpha f\eta_{\phi}}$. Conversely, if electron transfer is the rate-limiting step then $k_{CEPhT}\approx 2\pi k_{ET}\xi_{EDL}\mathrm{e}^{-(1-\alpha)fE^0}$. While these limits are in agreement with expectations from a sequential process with the presence of a rate-limiting step, it should be noted that they still include important physical insight related to EDL spillover, in the form of ξ_{EDL} .

To gain a deeper understanding of EDL spillover, we consider the case of a CEPhT reaction where the potential drop in the insulating phase is highly localized to the three-phase interface and the reaction is driven by a large overpotential ($f\eta_{\phi}\gg 1$) that brings the system to a mass-transport limited regime where the depletion of reactants at the interface is maximized, i.e., $C_{Fc}^{T}(R) = 0$. To simplify this treatment while maintaining agreement with FEM results, the potential at the PET in the toluene phase is approximated as an exponential decay with characteristic length scale λ^{-1} , i.e., $\eta'(r) \approx \eta_{\phi} \ \mathrm{e}^{-\lambda(r-R)}$. The concentration profile of (Fc)_{tol} along the PET is also approximated as an exponential, $h(r) \approx e^{-\beta(r-R)}$, with characteristic length scale β^{-1} . We should note that while both of these length scales are dependent on the geometry of the system, λ^{-1} is short (~2-3 nm) and depends on the electrostatic conditions at the three-phase interface, and β^{-1} is larger (~25 nm) and is determined by mass transport. In these conditions, $\xi_{EDL} \approx \alpha f \eta_{\phi} R / \lambda$. Together with the limiting cases above (which consider the value of k_{ET} and k_{PhT}), this result for ξ_{EDL} suggests that when CEPhT is driven by a large overpotential under strong confinement and in a mass-transport limited regime, the driving force is predicted to have a linear effect on k_{CEPhT} if limited by ET, but an exponential effect if limited by PhT. Considering that our experimental SECCM results show an exponential increase in current as the bias grows, these analytical calculations indicate that a phase-transfer limited sequential ET-PhT mechanism can explain our measurements. Efforts to control phase transfer in CEPhT by tuning the analyte's relative solubility in immiscible phases and the effect of voltametric scan rate are currently underway. Together with numerical FEM calculations that include a solvent mixing layer and a concerted mechanism, these analytical results identify the underlying EDL spillover phenomenon driving CEPhT and set the stage for future studies to probe the molecular-scale, dynamic events in this important class of reactions.

Conclusion

In summary, we propose an electrostatically-driven mechanism for the concerted CEPhT of Fc at the electrode/toluene/water (KCl) three-phase interface. FEM simulations reveal that EDL spillover from

the aqueous phase into an interfacial mixing region and the bulk toluene phase in proximity of the three-phase interface provides a sufficient electrostatic potential drop between the electrode surface and the PET in the toluene phase to drive Fc oxidation. A concerted CEPhT mechanism is proposed that occurs within ~1 nm of the three-phase interfacial boundary. Semiquantitative agreement between simulated and experimental voltammetry, combined with the predicted dependence of the *i-E* response on supporting electrolyte concentration supports EDL spillover as the origin of the electrochemical driving force. As the concentration of supporting electrolyte decreases and the aqueous phase EDL becomes more diffuse, (M-PET) at the three-phase boundary decreases and the driving force for CEPhT is lowered. The electrostatic model presented herein provides the fundamental basis for CEPhT at electrode/electrolyte/insulating-solvent interfaces where the extent of ET and PhT coupling can be investigated. Kinetic expressions for a sequential ET-PhT mechanism have been derived, providing the foundation to investigate the contributions of electron-transfer and phase-transfer kinetics in overall CEPhT reactivity. These results have implications for various multi-phase electrochemical applications where electron-transfer can be driven in classically forbidden phases including insulating solvents and gases.

Experimental Methods

Materials

Potassium chloride (ACS grade, Fisher Chemical), toluene (HPLC grade, VWR Chemicals), and hexaamineruthenium(III) chloride (Alfa Aesar) were used as obtained. Ferrocene (98%, Sigma-Aldrich) was purified by sublimation at ~95° C on a hotplate. All solutions were prepared with 18.2 M Ω cm deionized water obtained from a Barnstead Smart2Pure water purification system (Thermo Fisher Scientific).

Electrodes and Electrochemical Cell

A 3 mm GC electrode (CH Instruments, Inc.) was used as the substrate working electrode for all experiments. Prior to SECCM measurements, the GC electrode was polished with an aqueous slurry of 50 nm alumina particles on a cloth polishing pad (Buehler), rinsed with deionized water, and dried under ambient conditions. Ag/AgCl counter/reference wire electrodes were prepared by submerging a polished Ag wire (250 µm diameter) in bleach for over 20 minutes. Prior to SECCM measurements, the Ag/AgCl wire electrodes were rinsed extensively with deionized water and inserted into the quartz nanopipettes. All experiments were conducted using a home-built electrochemical cell with the glassy carbon electrode protruding through a Teflon baseplate (McMaster-Carr) into an open-top glass cylinder secured to the baseplate with a Viton O-ring. The GC electrode was secured between the baseplate and a backing plate by compressing an O-ring around the electrode sheath, forming a leak-proof cell. The Teflon electrochemical cell was rinsed with pure toluene between experiments and dried under ambient conditions.

Nanopipette Fabrication

Quartz nanopipettes were prepared using the laser-pulling method with a P-2000 laser puller (Sutter Instruments). A single-line pulling program (*Heat: 480, Filament: 3, Velocity: 30, Delay: 145, Pull: 175*) was used to generate a pair of nanopipettes from a quartz capillary with 1 mm outer diameter and 0.7 mm inner diameter (Sutter Instruments). This pulling procedure generated pipettes with radii on the order of 200-400 nm, measured from the resistive *i-E* response in 1 M KCl; see SI Section I. Nanopipettes were filled using Microfil 28G syringe tips (World Precision Instruments) and inspected by optical microscopy prior to SECCM measurements.

Scanning Electrochemical Cell Microscopy Measurements

SECCM measurements were conducted using a lab-built SECCM workstation controlled using the Warwick Electrochemical Scanning Probe Microscopy software suite.²⁴ The *z* position between the

26

nanopipette tip and the substrate electrode was controlled with a P-753.3CD piezoelectric stage (Physik

Instrumente, Karlsruhe Germany) controlled with a E-621 Piezo amplifier/ servo controller (Physik

Instrumente, Karlsruhe Germany). The x-y position of the nanoelectrochemical cell was controlled with a

NPYX200-101 dual-axis piezoelectric stage (nPoint, Inc.) using a LC.402 DSP Controller (nPoint, Inc.).

The current measured between the glassy carbon substrate electrode and an internal Ag/AgCl wire

reference/counter electrode was monitored using a Chem-Clamp amplifier (Dagan) and digitized using an

FPGA data acquisition card (PCIe-7852R, National Instruments). The current was measured at 2 kHz

sampling frequency and low pass filtered at 1 kHz prior to digitization. Subsequently, the measured signal

was downsampled to 78.125 Hz by averaging 256 data points. Voltammograms were digitally filtered

using a third-order Butterworth low-pass filter with a cutoff frequency of 5 Hz within MATLAB R2021a.

All voltammograms were plotted using Origin 2021b (OriginLab). For a given nanopipette, the average

and standard deviation of the i-E response were calculated from ~4-16 replicate measurements collected

in a hop-scan SECCM approach, wherein a new nanoelectrochemical meniscus cell is generated before

each voltammetric measurement.

Conflict of Interest Statement: The authors declare no competing interests.

Author Contributions: All authors have agreed to the final version of this manuscript.

Supporting Information

Online supporting information includes:

1. Supplementary Information File: I) Nanopipette Radii from Conductivity Measurements, II)

Voltammetric Characterization of Nanopipettes, III) Finite Element Method Simulation Details,

IV) Effect of Supporting Electrolyte Concentration on Electrochemical Microenvironment, V)

Electrolyte Dependence of EDL Spillover, VI) FEM Simulation Parametrization, VII) Analytical

Description of Sequential ET-PhT Mechanism, VIII) References.

2. COMSOL Model Report

Author Information

Corresponding Authors

Henry S. White – Department of Chemistry, University of Utah, Salt Lake City, Utah 84112, United States; https://orcid.org/0000-0002-5053-0996; Email: white@chemistry.utah.edu

Rodrigo Noriega - Department of Chemistry, University of Utah, 315 S. 1400 E, Salt Lake City, Utah 84112, United States; http://orcid.org/0000-0003-1199-0866; Email: noriega@chem.utah.edu

Authors

Andrew D. Pendergast - Department of Chemistry, University of Utah, Salt Lake City, Utah 84112, United States; https://orcid.org/0000-0003-3311-1260

Salvador Gutierrez-Portocarrero – Department of Chemistry, University of Utah, Salt Lake City, Utah, 84112, United States; https://orcid.org/0000-0002-9154-2790

Acknowledgments: This work was funded by the National Science Foundation (NSF-CHE-2300863) and the Office of Naval Research (N00014-22-1-2425). ADP acknowledges support from the National Science Foundation Graduate Research Fellowship under Grant No. 1747505.

References

- 1. Clarke, T. B.; Colón, G. S.; Dick, J. E., Tunable Gold Nanoring Arrays by Electrodeposition. *Advanced Materials Technologies* **2023**, *8* (13), 2201946.
- 2. Reyes-Morales, J.; Dick, J. E., Electrochemical-Shock Synthesis of Nanoparticles from Sub-Femtoliter Nanodroplets. *Accounts of Chemical Research* **2023**, *56* (10), 1178-1189.
- 3. Koper, M. T. M.; Schmickler, W., A Theory for Amalgam Forming Electrode Reactions. *Journal of Electroanalytical Chemistry* **1998**, *450* (1), 83-94.
- 4. Daviddi, E.; Shkirskiy, V.; Kirkman, P. M.; Robin, M. P.; Bentley, C. L.; Unwin, P. R., Screening the Surface Structure-Dependent Action of a Benzotriazole Derivative on Copper Electrochemistry in a Triple-Phase Nanoscale Environment. *Journal of Physical Chemistry C* **2022**, *126* (35), 14897-14907.

- 5. Daviddi, E.; Shkirskiy, V.; Kirkman, P. M.; Robin, M. P.; Bentley, C. L.; Unwin, P. R., Nanoscale Electrochemistry in a Copper/Aqueous/Oil Three-Phase System: Surface Structure-Activity-Corrosion Potential Relationships. *Chemical Science* **2021**, *12* (8), 3055-3069.
- 6. Yuan, H.; Peng, H. J.; Li, B. Q.; Xie, J.; Kong, L.; Zhao, M.; Chen, X.; Huang, J. Q.; Zhang, Q., Conductive and Catalytic Triple-Phase Interfaces Enabling Uniform Nucleation in High-Rate Lithium-Sulfur Batteries. *Advanced Energy Materials* **2019**, *9* (1), 1802768.
- 7. Luck, J.; Latz, A., Modeling of the Electrochemical Double Layer and Its Impact on Intercalation Reactions. *Physical Chemistry Chemical Physics* **2018**, *20* (44), 27804-27821.
- 8. Itagaki, R.; Takizawa, S. Y.; Chang, H. C.; Nakada, A., Light-Induced Electron Transfer/Phase Migration of a Redox Mediator for Photocatalytic C-C Coupling in a Biphasic Solution. *Dalton Transactions* **2022**, *51* (24), 9467-9476.
- 9. Zhou, H.; Sheng, X.; Ding, Z. Y.; Chen, X.; Zhang, X. Q.; Feng, X. J.; Jiang, L., Liquid-Liquid-Solid Triphase Interface Microenvironment Mediates Efficient Photocatalysis. *Acs Catalysis* **2022**, *12* (21), 13690-13696.
- 10. Marcus, R. A., Chemical + Electrochemical Electron-Transfer Theory. *Annual Review of Physical Chemistry* **1964**, *15*, 155-&.
- 11. Benjamin, I., Structure, Thermodynamics, and Dynamics of Thiocyanate Ion Adsorption and Transfer across the Water/Toluene Interface. *Journal of Physical Chemistry B* **2022**, 126 (30), 5706-5714.
- 12. Tasakorn, P.; Chen, J. Y.; Aoki, K., Voltammetry of a Single Oil Droplet on a Large Electrode. *Journal of Electroanalytical Chemistry* **2002**, *533* (1-2), 119-126.
- 13. Chen, J. Y.; Ikeda, O.; Aoki, K., Electrode Reaction of Ferrocene in a Nitrobenzene Plus Water Emulsion. *Journal of Electroanalytical Chemistry* **2001**, *496* (1-2), 88-94.
- 14. Bak, E.; Donten, M.; Stojek, Z., Three-Phase Electrochemistry with a Cylindrical Microelectrode. *Electrochemistry Communications* **2005**, *7* (5), 483-489.
- 15. Weatherly, C. K. T.; Ren, H.; Edwards, M. A.; Wang, L.; White, H. S., Coupled Electron- and Phase-Transfer Reactions at a Three-Phase Interface. *Journal of the American Chemical Society* **2019**, *141* (45), 18091-18098.
- 16. Ebejer, N.; Schnippering, M.; Colburn, A. W.; Edwards, M. A.; Unwin, P. R., Localized High Resolution Electrochemistry and Multifunctional Imaging: Scanning Electrochemical Cell Microscopy. *Analytical Chemistry* **2010**, *82* (22), 9141-9145.
- 17. Wu, J. S.; Toda, K.; Tanaka, A.; Sanemasa, I., Association Constants of Ferrocene with Cyclodextrins in Aqueous Medium Determined by Solubility Measurements of Ferrocene. *Bulletin of the Chemical Society of Japan* **1998**, *71* (7), 1615-1618.
- 18. Bard, A. J.; Faulkner, L. R.; White, H. S., *Electrochemical Methods: Fundamentals and Applications, 3rd Edition.* Wiley: 2022.
- 19. He, R.; Chen, S. L.; Yang, F.; Wu, B. L., Dynamic Diffuse Double-Layer Model for the Electrochemistry of Nanometer-Sized Electrodes. *Journal of Physical Chemistry B* **2006**, *110* (7), 3262-3270.
- 20. Bockris, J. O.; Devanathan, M. A. V.; Muller, K., On Structure of Charged Interfaces. *Proceedings of the Royal Society of London Series a-Mathematical and Physical Sciences* **1963**, 274 (1356), 55-+.
- 21. Neumaier, L.; Schilling, J.; Bardow, A.; Gross, J., Dielectric Constant of Mixed Solvents Based on Perturbation Theory. *Fluid Phase Equilibria* **2022**, *555*, 113346.
- 22. Dunitz, J. D.; Orgel, L. E.; Rich, A., The Crystal Structure of Ferrocene. *Acta Crystallographica* **1956**, *9* (4), 373-375.
- 23. Cooper, J. B.; Bond, A. M.; Oldham, K. B., Microelectrode Studies without Supporting Electrolyte Model and Experimental Comparison for Singly and Multiply Charged Ions. *Journal of Electroanalytical Chemistry* **1992**, *331* (1-2), 877-895.

24. Ebejer, N.; Güell, A. G.; Lai, S. C. S.; McKelvey, K.; Snowden, M. E.; Unwin, P. R., Scanning Electrochemical Cell Microscopy: A Versatile Technique for Nanoscale Electrochemistry and Functional Imaging. *Annual Review of Analytical Chemistry* **2013**, *6* (1), 329-351.

Coupled Electron- and Phase-Transfer

